Sensitivity of the North Atlantic Ocean Circulation to an Abrupt Change in the Nordic Sea Overflow in a High Resolution Global Coupled Climate Model

Rong Zhang[1], Thomas L. Delworth[1], Anthony Rosati[1], Whit G. Anderson[1], Keith W. Dixon[1], Hyun-Chul Lee[1,2], and Fanrong Zeng[1]

[1]GFDL/NOAA, Princeton, NJ, USA

[2]High Performance Tech. Inc. Reston, Virginia, USA

Rong Zhang, GFDL/NOAA, Princeton, New Jersey, 08540, (Rong.Zhang@noaa.gov)

The sensitivity of the North Atlantic Ocean Circulation to an abrupt change in the Nordic Sea overflow is investigated for the first time using a high resolution eddy-permitting global coupled ocean-atmosphere model (GFDL CM2.5). The Nordic Sea overflow is perturbed through the change of the bathymetry in GFDL CM2.5. We analyze the Atlantic Meridional Overturning Circulation (AMOC) adjustment process and the downstream oceanic response to the perturbation. The results suggest that in the region north of 34°N, AMOC changes induced by changes in the Nordic Sea overflow propagate on the slow tracer advection time scale, instead of the fast Kelvin wave time scale, resulting in a time lead of several years between subpolar and subtropical AMOC changes. The results also show that a stronger and deeper-penetrating Nordic Sea overflow leads to stronger and deeper AMOC, stronger northward ocean heat transport, reduced Labrador Sea deep convection, stronger cyclonic Northern Recirculation Gyre (NRG), westward shift of the North Atlantic Current (NAC) and southward shift of the Gulf Stream, warmer sea surface temperature (SST) east of Newfoundland and colder SST south of the Grand Banks, stronger and deeper NAC and Gulf Stream, and stronger oceanic eddy activities along the NAC and the Gulf Stream paths. This sensitivity study points to the important role of the Nordic Sea overflow in the large scale North Atlantic ocean circulation, and it is crucial for climate models to have a correct representation of the Nordic Sea overflow.

1. Introduction

The Nordic Sea overflow, which enters into the deep North Atlantic through the Greenland-Iceland-Scotland (GIS) ridge, is one of the major sources for the North Atlantic Deep Water (NADW) and contributes significantly to the deep branch of the Atlantic Meridional Overturning Circulation (AMOC). The impact of the southward NADW outflow on the North Atlantic ocean circulation has been studied previously using coarse resolution climate models. For example, some modeling studies suggest that a stronger NADW outflow, and thus a stronger AMOC, leads to a strengthening of the cyclonic Northern Recirculation Gyre (NRG) and a southward shift of the Gulf Stream path [Gerdes and Köberle, 1995; Zhang and Vallis, 2007; Zhang, 2008; Yeager and Jochum, 2009]. While these modeling results are consistent with the observations at Line W [Peña-Molino and Joyce 2008; Joyce and Zhang, 2010; Toole et al. 2010], some other ocean-only hindcast models [de Coẽtlogon et al. 2006] suggest the opposite, i.e. a stronger NADW outflow, and thus a stronger AMOC, leads to a northward shift of the Gulf Stream path.

In many climate models, the simulated Nordic Sea overflow entering into the deep North Atlantic through the GIS ridge is unrealistically weak, compared to the observation [Dickson et al. 1990]. This bias is mainly caused by excessive convective entrainment of the overflow over staircase bathymetry in the climate models, leading to much lighter and shallower overflow waters [Winton et al. 1998; Danabasoglu et al. 2010]. Danabasoglu et al. [2010] proposed a new physical parameterization for the Nordic Sea overflow, and studied the impact of the Nordic Sea overflow parameterizations on the North Atlantic ocean circulation in a coupled coarse resolution climate model (NCAR CCSM4) as well as in its uncoupled ocean component. In both the coupled and uncoupled ocean-only simulations, Danabasoglu et al. [2010] found that a stronger and deeper Nordic Sea overflow leads to a northward shift of the Gulf Stream path and a further weakening of the cyclonic NRG. All these previous coarse resolution model simulations lack explicit oceanic eddy activities and have broader western boundary currents than observed, and some ocean-only models do not have realistic air-sea boundary conditions. Hence it is important to reinvestigate the linkage between the NADW outflow and the North Atlantic ocean circulation using higher resolution coupled models.

The response of the North Atlantic ocean circulation to changes in the NADW is established through the transient adjustment process. The AMOC adjustment process to an abrupt change in the northern high latitudes is often thought to be through the propagation of fast Kelvin waves, based on the classic picture that the NADW outflow moves along the western boundary as DWBC [Kawase, 1987; Johnson and Marshall, 2002]. The fast Kelvin wave will lead to an almost in-phase relationship between high and low latitudes AMOC changes. However, recent observations with acoustically tracked Range and Fixing of Sound (RAFOS) floats [Bower et al. 2009] show that the a significant part of the NADW does not move along the western boundary, but actually along interior pathways from Flemish Cap to Cape Hatteras. Zhang [2010] shows that the existence of interior pathways of NADW causes a fundamentally different AMOC propagation mechanism, i.e. AMOC variations estimated in density space propagate on the slow tracer advection time scale due to the existence of interior pathways of NADW from Flemish Cap to Cape Hatteras, resulting in a much longer time lead (several years) between subpolar and subtropical AMOC variations. The longer time lead provides a more useful predictability. However, the above study is based on a coarse resolution coupled climate model (GFDL CM2.1), which lacks explicit eddies, has broaden boundary currents and weaker deep western boundary current (DWBC) from Flemish Cap to Cape Hatteras than that observed, and slows down the Kelvin wave artificially. Hence it is necessary to reinvestigate the AMOC adjustment process to an abrupt change in the northern high latitudes using higher resolution coupled models.

In this paper, we study the sensitivity of the North Atlantic ocean circulation to an abrupt change in the Nordic Sea overflow for the first time using a high resolution eddy-permitting global coupled ocean-atmosphere model CM2.5. The model is recently developed at Geophysical Fluid Dynamics Laboratory (GFDL) [Delworth et al., manuscript in preparation, 2011]. In this sensitivity study, we focus on the AMOC adjustment process and downstream oceanic response to an abrupt change in the Nordic Sea overflow. The strength of the Nordic Sea overflow in climate models is very sensitive to changes in the model bathymetry [Roberts and Wood, 1997]. In this study, we perturb the Nordic Sea overflow by modifying the bathymetry in CM2.5. Our results suggest that in the region north of 34°N, AMOC changes induced by the abrupt change in the Nordic Sea overflow propagate on the slow tracer advection time scale, instead of the fast Kelvin wave time scale, resulting in a time lead of several years between subpolar and subtropical AMOC changes.

Many climate model simulations show common large scale biases in the North Atlantic ocean circulation, such as the large scale SST biases associated with the biases of the northward shift of the Gulf Stream path and the eastward shift of the NAC path [Weese and Bryan, 2006; Bryan et al. 2007; Molinari et al. 2008]. The Gulf Stream has a significant influence on the troposphere [Minobe et al., 2008]. Changes in the path of the Gulf Stream can force significant changes in the synoptic wintertime atmospheric variability [Joyce et al., 2009]. The typical biases in the NAC path will also lead to biases of the water mass properties in the subpolar North Atlantic and the Nordic Seas [Weese and Bryan, 2006]. Here our high resolution eddy-permitting coupled modeling results also show that a stronger and deeper-penetrating Nordic Sea overflow leads to a stronger cyclonic NRG, a southward shift of the Gulf Stream, and a westward shift of the NAC, as well as many other large scale changes in the North Atlantic ocean circulation that are opposite to the common biases in climate model simulations.

2. Description of the High Resolution Coupled Ocean-Atmosphere Model and Experiments

The high resolution coupled model used here (GFDL CM2.5) will be described in a detailed documentation [Delworth et al., manuscript in preparation, 2011]. The ocean component is based on MOM4p1 [Griffies, 2010] and has 50 vertical levels (22 levels of 10-m thickness each in the top 220 m), and the horizontal resolution is eddy-permitting, varying from $1/4^{\circ}$ (or 27.75 km) at the equator to 9 km at high latitudes with a squared isotropic grid. Prognostic tracers are advected by the multi-dimensional piecewise parabolic scheme (MDPPM). It has very small viscosity from the biharmonic Smagorinsky scheme, with no parameterization for explicit diffusion, in order to reproduce energetic and realistic frontal and eddy structures. The resolution of the atmosphere component is also increased to 32 levels in the vertical, and 50km in the horizontal with a finite volume dynamical core on cubed sphere grids [Putman and Lin, 2007]. The model has similar atmospheric physics to that employed in the coarse resolution coupled model GFDL CM2.1 [Delworth et al. 2006]. CM2.5 also employs a new land model LM3.

The control experiment uses the 1990 radiative forcing conditions and produces a stable integration for 280 years without flux adjustments. The solution is quite realistic in general [Delworth et al., manuscript in preparation, 2011]. However, even with the high resolution eddy-permitting ocean grids and with the artificially deepened Denmark Strait depth (926m) in the control experiment, the simulated Nordic Sea overflow entering into the deep North Atlantic through the Greenland-Iceland-Scotland (GIS) ridge is still unrealistically weak (about 2 Sv), compared to the observed value of about 5-6 Sv [Dickson et al. 1990]. This bias is mainly caused by excessive convective entrainment of the overflow over staircase bathymetry in the model, leading to much lighter and shallower overflow waters [Winton et al. 1998; Danabasoglu et al. 2010].

Roberts and Wood [1997] show that the simulated strength of the Nordic Sea overflow is very sensitive to changes in the model bathymetry. To study the sensitivity of the North Atlantic ocean circulation to the abrupt change of the Nordic Sea overflow, we conduct a perturbed experiment (P1) for 20 years in which the bathymetry south of the Denmark Strait is deepened by 300m (Fig. 1 a,b), whenever the background ocean depth in this area in the control experiment (C1) is more than 300m. With this modification of the bathymetry, the downstream pathways of the Nordic Sea overflow (in particular the Denmark Strait overflow) are deepened and widened, resulting in an instantaneous strengthening and deeper penetration of the Nordic Sea overflow in the deep ocean south of the Denmark Strait.

In this paper, we study the AMOC adjustment process to the abrupt change in the Nordic Sea overflow using the first 10 years of the control (C1) and perturbed (P1) experiments. In addition, another set of control (C2) and perturbed (P2) experiments are conducted for several decades, with the bathymetry south of the entire GIS Ridge deepened by 300m in the perturbed experiment (P2), whenever the background ocean depth in this area in the control experiment (C2) is more than 300m (Fig. 1 c,d). With a larger area of deepening, the instantaneous strengthening of the Nordic Sea overflow in the deep ocean south of the GIS Ridge in P2 is larger than that in P1. We also analyze the AMOC adjustment process using the first 10 years of experiments C2 and P2 to check the robustness of the results found with experiments C1 and P1. There are some minor localized bathymetry difference between C2/P2 and C1/P1 near the Florida Strait and the Indonesian Archipelago.

In this paper, we also study the impact of the Nordic Sea overflow on the North Atlantic ocean circulation by focusing our analyses on the results averaged from year 6 to 10 of the control (C1) and perturbed (P1) experiments respectively. The results from C2 and P2 are similar and not shown. As will be discussed in detail in the following section, the abrupt strengthening of the Nordic Sea overflow in the perturbed experiment starts to have a significant impact on the North Atlantic ocean circulation at lower latitudes south of the Grand Banks at around year 5. Hence we analyze the impact on the North Atlantic ocean circulation using modeling results after the first 5 years. On the other hand, although the Nordic Sea overflow instantaneously adopts a large value after modifying the bathymetry in the perturbed experiment, it gradually weakens afterwards in association with the reduction of the density of the Nordic Sea source water as will be discussed in detail in section 4. The associated downstream impacts on the North Atlantic ocean circulation are also reduced in time with the weakening of the Nordic Sea overflow. Hence we choose the average of year 6 to 10 of the control (C1) and perturbed (P1) experiments for our analyses of the impact on the North Atlantic ocean circulation because the impact is still significantly strong during this early period.

3. Sensitivity of the North Atlantic Ocean Circulation to an Abrupt Change in the Nordic Sea Overflow

3.1. AMOC Adjustment Process

The modification of the bathymetry in the perturbed experiment (P1) leads to an instantaneous strengthening and deeper penetration of the Nordic Sea overflow in the deep ocean south of the Denmark Strait. The abrupt change in the Nordic Sea overflow then triggers an anomalous southward deep flow which reaches the equator along the western boundary within 1 year due to the initial fast Kelvin wave adjustment (Fig. 2a). However, the anomalous southward deep flow near the western boundary, especially the one at south of the Grand Banks, is still much weaker at year 1 and becomes much stronger only after several years (Fig. 2a,b).

The difference of the Atlantic overturning streamfunction between the perturbed (P1) and control (C1) experiments is largest at the constant potential density level $1036.9kg/m^3$. Fig. 3a shows AMOC changes $(P1-C1)$ at this constant density level as a function of latitude for the first 10 years. The relative AMOC changes (Fig. 3b), i.e. $(P1-C1)$ minus the 10-year mean difference $(\overline{P1}-\overline{C1})$ at each latitude, shows more clearly that AMOC changes propagate southward, and AMOC changes at the subtropics lag those at the northern high latitudes by several years. Results from another set of perturbed (P2) and control (C2) experiments show a very similar pattern of the AMOC adjustment (Fig. 3b,d), and the AMOC response is even stronger due to a larger bathymetry perturbation in P2. In both sets of experiments, AMOC changes show a significant southward tilt with time in the region north of 34°N. From south of 34°N to the equator, AMOC changes at various latitudes are almost in phase. This AMOC propagation characteristics is very similar to that found with the coarse resolution coupled model (GFDL CM2.1) [Zhang, 2010].

The several-year time lag between AMOC changes at the subtropics and AMOC changes at the high latitudes is inconsistent with the fast Kelvin wave adjustment, but consistent with the slow tracer advection time scale in the region north of 34°N. Fig. 4 a,b,c shows the distribution of the annual mean passive dye tracer at the deep ocean of year 2,4,6 respectively in the perturbed experiment (P1). The passive dye tracer is released continuously from the Denmark Strait (at the depth from 572m to 926m) with a constant concentration of 1. The passive dye tracer propagates to lower latitudes near the western boundary and gradually reaches the western North Atlantic basin south of the Grand Banks after several years due to the advection by the mean deep current (Fig. 4a,b,c). The southwestward propagation of the passive dye tracer released from the Denmark Strait can also be seen in more details from the 3-dimensional animation for year 1 to 10 of the perturbed experiment P1 (Animation 1).

In the region north of 34°N, a significant part of the deep flow moves along interior pathways near the western boundary (Fig. 2b) even in this high resolution eddy-permitting model, i.e. the deep flow is not confined completely to the thin layer along the western boundary as it does south of 34°N. The simulated interior pathways of NADW are consistent with that observed recently using acoustically tracked Range and Fixing of Sound (RAFOS) floats [Bower et al., 2009]. Due to the existence of the interior pathways, the adjustment of AMOC changes in the region north of 34°N is in two stages. The initial stage is the fast Kelvin wave response, and the signal carried by the Kelvin wave adjustment is very weak (Fig. 2a). In the second stage, a significant part of the deep flow anomaly moves along interior pathways with the density anomaly that is advected by the mean NADW outflow along interior pathways, and it can not propagate with the fast Kelvin wave in the interior ocean. When a positive southward deep flow anomaly moves along interior pathways with the slow tracer advection time scale, it interacts with the bottom topography and induces a positive bottom vortex stretching anomaly (downslope), thus strengthening the barotropic cyclonic gyre [Zhang and Vallis, 2007; Zhang, 2010]. Hence the barotropic cyclonic gyre propagates southwestward from the subpolar region into the region south of the Grand Banks on the same tracer advection time scale (Fig.4 d,e,f). When the cyclonic gyre propagates to south of the Grand Banks a few years later, it strengthens the DWBC and pushes the Gulf Stream path southward. Hence the changes of the DWBC, as well as changes of the AMOC (include both the DWBC and the interior deep flow) propagate on the same tracer advection time scale.

In the region from south of 34°N to the equator, the deep meridional flow anomaly moves mainly along the western boundary, not through interior pathways (Fig. 2b). Hence the AMOC adjustment in this region is simply through the fast Kelvin wave process and AMOC changes at various latitudes in this region are almost in phase.

In summary, in this high resolution eddy-permitting model GFDL CM2.5, the simulated two-stage AMOC adjustment process in the region north of 34°N, as well as the in-phase relationship of AMOC changes from south of 34°N to the equator, are very similar to that found with the coarse resolution coupled model (GFDL CM2.1) [Zhang, 2010]. The consistency between the high and low resolution coupled models suggests that the simulated AMOC propagation and adjustment process are robust. In particular, the AMOC adjustment process between the subpolar and the subtropical region is dominated by the slow tracer advection process, instead of the fast Kelvin wave response.

3.2. Impact on the North Atlantic Ocean Circulation

We now analyze the impact of the Nordic Sea overflow on the North Atlantic ocean circulation using results averaged from year 6 to 10 of the control (C1) and perturbed (P1) experiments respectively. The results from C2 and P2 are similar and not shown. In the control experiment (C1), the Nordic Sea overflow entered into the North Atlantic deep ocean is very weak (Fig. 5a,c). Hence the downstream deep flow near the western boundary is also very weak. Part of deep flow moves eastward near 50°N, and some moves further southward in the interior ocean near the Mid Atlantic Ridge, resulting in an eastward distribution of the younger age tracer and the passive dye tracer released from the Demark Strait in the interior ocean (Fig. 5a,c). Due to the lack of a strong deep flow near the western boundary south of the Flemish Cap, the younger age tracer and the passive dye tracer released from the Demark Strait are mainly confined to the subpolar region and do not penetrate south of the Grand Banks (Fig. 5 a,c). The detailed spatial distribution of the passive dye tracer released from the Denmark Strait can also be seen from the 3-dimensional animation for year 1 to 10 of the control experiment C1 (Animation 2). On the contrary, in the perturbed experiment (P1), when a much stronger Nordic Sea overflow enters into the North Atlantic deep ocean through the Denmark Strait, the downstream deep flow near the western boundary is also much stronger, even in regions south of the Grand Banks (Fig. 5 b,d). Hence the younger age tracer and the passive dye tracer released from the Denmark Strait show much higher concentration near the western boundary and less eastward distribution in the interior ocean, and can reach the western North Atlantic basin south of the Grand Banks due to the advection by the deep flow (Fig. 5 b,d; Animation 1).

In the perturbed experiment (P1), the total transport of the Nordic Sea overflow water (with the neutral density from 27.975 to 28.14 kg/m^3) across the GIS Ridge is increased to about 5 Sv from about 2 Sv in the control experiment (C1). The zero contour line of the annual mean Atlantic meridional overturning streamfunction at 35°N is deepened to about 4000m from 3000m in the control experiment C1 (Fig. 6). The maximum annual mean AMOC at 26.5°N is increased to about 18 Sv (from 15 Sv in the control experiment C1) (Fig. 6), similar to that found in the direct observation using RAPID arrays [Cunningham et al. 2007; Kanzow et al. 2010]. The annual mean northward ocean heat transport at 24°N is enhanced to 1.16 PW (from 0.99 PW in the control experiment C1), consistent with that estimated from the World Ocean Circulation Experiment (WOCE) hydrographic section at 24°N [Lumpkin and Speer 2007]. As expected, the stronger Nordic Sea overflow advects colder and fresher Nordic Sea water into the deep subpolar North Atlantic and downstream near the western boundary. The annual mean Mixed Layer Depth (MLD) in the Labrador Sea is also reduced by about 400m compared to that in the control experiment (C1) due to enhanced vertical stratification induced by the dense Nordic Sea overflow water entering the deep Labrador Sea basin. The above results are consistent with those found in the coarse resolution coupled model (NCAR CCSM4) with an explicit parameterization of the Nordic Sea overflow [Danabasoglu et al., 2010].

In the perturbed experiment (P1), the stronger NADW outflow around the Flemish Cap and the Grand Banks shifts westward and moves not only along the western boundary as the DWBC, but also downslope along interior pathways just off the western boundary (Fig. 5b,d), similar to that observed recently [Bower et al. 2009]. As mentioned in Section 3.1, the stronger downslope deep flow along interior pathways interacts with the steep continental slope, inducing stronger positive bottom vortex stretching thus stronger cyclonic barotropic gyre near the western boundary off the Flemish cap, south of the Grand Banks and downstream to Cape Hatteras after the several-year advection adjustment process, in comparison to that in the control experiment C1 (Fig. 7a,b). Hence the North Atlantic Current (NAC) path is shifted westward, the cyclonic NRG north of the Gulf Stream is stronger, and the Gulf Stream path is shifted southward, compared to that in the control experiment C1 (Fig. 7a,b).

The above relationship, i.e. a stronger southward NADW outflow (thus a stronger AMOC) vs. a westward shift of the NAC path, a stronger cyclonic NRG and a southward shift of the Gulf Stream path, is consistent with that found in some coarse resolution modeling studies [Gerdes and Köberle, 1995; Zhang and Vallis, 2007; Zhang, 2008; Yeager and Jochum, 2009], but opposite to that found in the ocean-only coarse resolution simulation [de Coẽtlogon et al. 2006]. Changes in the cyclonic barotropic gyre circulation induced by changes in the deep flow are less broad in this eddy-permitting high resolution model than in those coarse resolution models. The simulated relationship between a stronger NADW outflow and a southward Gulf Stream path is also consistent with recent observations at Line W [Peña-Molino and Joyce 2008; Joyce and Zhang, 2010; Toole et al. 2010].

In the control experiment C1 the unrealistic eastward shift of the NAC path leads to a large area of cold SST east of Newfoundland, meanwhile the very weak cyclonic NRG and the northward shift of the Gulf Stream path lead to a warm SST south of the Grand Banks (Fig. 7a,c), both are common issues in climate model simulations [Weese and Bryan, 2006; Bryan et al. 2007; Molinari et al. 2008]. In the perturbed experiment P1, changes in the barotropic gyre circulation and the associated westward shift of the NAC path and the southward shift of the

Gulf Stream path lead to much warmer SST east of Newfoundland and colder slope water south of the Grand Banks (Fig. 7b,d; Fig. 8). In the perturbed experiment (P1), the simulated Gulf Stream and NAC not only shift their paths, but also are much stronger in strength and reach much deeper in depth with more enhanced barotropic components (Fig. 9).

Changes in ocean currents also lead to changes in ocean eddy activities. The strongest Eddy Kinetic Energy (EKE) of the surface geostrophic flow and the rms sea surface height (SSH) variability appear along the major current paths (Fig. 10). In the control experiment (C1), the region with the strongest EKE and SSH variability is located too far east at mid latitudes due to the eastward shift of the NAC (Fig. 10 a,d). In the perturbed experiment (P1), the eddy activities are much stronger along the Gulf Stream and NAC paths, and the region with the strongest EKE and SSH variability shifts westward with the NAC at mid latitudes, turns to the northwest after passing the Flemish Cap and forms the "northwest corner" (Fig. 10 b,e), similar to the observed pattern using altimetry data (Fig. 10 c,f). The amplitudes of the EKE and SSH variability in the perturbed experiment (P1) using this eddy-permitting model are still smaller than observed, and higher resolution (eddy-resolving) models have been shown to be capable to simulate the observed amplitudes [Smith et al. 2000; Bryan et al. 2007; Hecht and Smith, 2008].

4. Conclusion and Discussion

In this sensitivity study, we investigate the AMOC adjustment process and downstream oceanic response to an abrupt change in the Nordic Sea overflow for the first time using a high resolution eddy-permitting global coupled ocean-atmosphere model (GFDL CM2.5). Previous studies on similar subjects often use coarse resolution models, which lack explicit oceanic eddy activities and have broader western boundary currents than observed, and some ocean-only models do not have realistic air-sea boundary conditions. Here our modeling results using a high resolution eddy-permitting global coupled ocean-atmosphere model (GFDL CM2.5) show that in the region north of 34°N, due to the existence of interior pathways, AMOC changes induced by an abrupt change in the Nordic Sea overflow propagate on the slow tracer advection time scale, instead of the fast Kelvin wave time scale. The slow advection time scale results in a time lead of several years between subpolar and subtropical AMOC changes, consistent with that found in the coarse resolution model GFDL CM2.1 [Zhang, 2010]. The barotropic cyclonic gyre propagates southwestward with the same tracer advection time scale. When the cyclonic gyre propagates to south of the Grand Banks several years later, it strengthens the DWBC and pushes the Gulf Stream path southward. In the region from south of 34°N to the equator, the deep meridional flow anomaly moves mainly along the western boundary, not through interior pathways. Hence the AMOC adjustment in this region is simply through the fast Kelvin wave process and AMOC changes at various latitudes in this region are almost in phase.

Our modeling results also show that the Nordic Sea overflow has a significant impact on the North Atlantic ocean circulation. For example, a stronger and deeper-penetrating Nordic Sea overflow will lead to stronger and deeper AMOC, stronger northward ocean heat transport, reduced Labrador Sea deep convection, stronger cyclonic NRG, westward shift of the NAC and southward shift of the Gulf Stream, warmer SST east of Newfoundland and colder SST south of the Grand Banks, stronger and deeper NAC and Gulf Stream, and stronger eddy activities along the NAC and the Gulf Stream paths. Our modeling results suggest that the relationship between a stronger Nordic Sea overflow (thus a stronger AMOC) vs. a westward shift of the NAC path, a stronger cyclonic NRG and a southward shift the Gulf Stream path, is robust even with the presence of explicit eddy activities.

This sensitivity study points to the important role of the Nordic Sea overflow in the large scale North Atlantic ocean circulation. The results suggest that the lack of a well-simulated Nordic Sea overflow will lead to many large scale biases in the North Atlantic ocean circulation which are common in many model simulations, such as the large scale SST biases associated with the biases in the paths of the Gulf Stream and the NAC [Weese and Bryan, 2006; Bryan et al. 2007; Molinari et al. 2008]. The atmosphere circulation and the long term climate are sensitive to the paths of the Gulf Stream and the NAC [Weese and Bryan, 2006; Minobe et al., 2008; Joyce et al., 2009]. Hence it is crucial for climate models to have a correct representation of the Nordic Sea overflow, so as to have a realistic simulation of the North Atlantic ocean circulation.

In both perturbed (P1) and control (C1) experiments, the surface water in the interior Nordic Sea becomes much lighter by year 16 to 20 (Fig. 11). We speculate that this is because the simulated warm salty upper North Atlantic water transported into the Nordic Sea is mainly confined to the eastern boundary of the Nordic Sea or even leaked into the Barents Sea, and not efficiently mixed into the interior Nordic Sea within a decade to maintain the surface density there. Hence in the perturbed experiment (P1), although the Nordic Sea overflow instantaneously adopts a large value after modifying the bathymetry, it is gradually reduced afterwards with the lighter Nordic Sea source water. The North Atlantic ocean circulation is very sensitive to the change in the Nordic Sea overflow, i.e. all the associated downstream impacts on the North Atlantic ocean circulation are reduced with the weakening of the Nordic Sea overflow. In the perturbed experiment (P1), the increase of surface density along the east coast of Greenland by year 16 to

20 (Fig. 11, compared to year 6 to 10) is due to the weakening of the east Greenland current in response to the continuous weakening of the Nordic Sea overflow, so that less fresh water is transported from the Arctic to the east coast of Greenland and the surface density is gradually increased there.

It is possible that the impact shown in this paper is a transient response to the transient enhancement of the Nordic Sea overflow. A physical parameterization of the Nordic Sea overflow as described in Danabasoglu et al. [2010] is being implemented in GFDL CM2.5, and the preliminary results show that the parameterized Nordic Sea overflow has a very similar impact as that shown in this paper. For the short period of simulation presented in this paper, it is not possible to assess the impact of the Nordic Sea overflow on the AMOC variability and on the atmosphere circulation and long term climate. We will investigate the equilibrated response to the Nordic Sea overflow, its impact on the AMOC variability, and its impact on the atmosphere circulation and long term climate in the near future, once we simulate a realistic strong Nordic Sea overflow over a much longer period with the overflow parameterization.

In the perturbed experiment the Nordic Sea overflow is dominated by the Denmark Strait overflow, and the Faroe Bank Channel (FBC) overflow is not resolved. This is a caveat of this study. How to simulate and maintain the observed structure and strength of the Nordic Sea overflow is beyond the scope of this study. On the other hand, in reality both the Denmark Strait overflow and the FBC overflow move to the downstream deep Labrador Sea basin and would have similar downstream impacts further southward. For climate model development, a realistic simulation of the Nordic Sea overflow should be obtained by explicit parameterization instead of changing the bathymetry. However, in this sensitivity study we focus on the downstream oceanic adjustment and response to an abrupt change in the Nordic Sea overflow, and we perturb the Nordic Sea overflow by modifying the bathymetry. We expect similar impacts would occur if we had perturbed the Nordic Sea overflow by some other approaches, such as perturbing the density of the Nordic Sea surface water.

Acknowledgments

We thank Mike Winton and Geoff Vallis for the very helpful suggestions on an earlier version of the paper. We thank Simon Su at GFDL for constructing the 3-dimensional animations of the passive dye tracer presented in the paper.

Reference

Bower, A. S., M. S. Lozier, S. F. Gary, and C. W. Böning (2009), Interior pathways of the North Atlantic meridional overturning circulation. *Nature*, **459** 243-248; DOI: 10.1038/nature07979.

Cunningham et al. (2007), Temporal Variability of the Atlantic Meridional Overturning Circulation at 26.5°N. *Science*, **317**, 935-938.

Danabasoglu, G., W. G. Large, and B. P. Briegleb (2010), Climate impacts of parameterized Nordic Sea overflows, *J. Geophys. Res.*, **115**, C11005, doi:10.1029/2010JC006243.

de Coëtlogon, G., C. Frankignoul, M. Bentsen, C. Delon, H. Haak, S. Masina, and A. Pardaens (2006), Gulf Stream Variability in Five Oceanic General Circulation Models. *J. Phys. Oceanogr.*, **36**, 2119-2135.

Delworth et al. 2006, GFDL's CM2 Global Coupled Climate Models. Part I: Formulation and Simulation Characteristics. *J. Climate*, **19**, doi:10.1175/JCLI3629.1.

Dickson, R. R., E. M. Gmitrowicz, and A. J. Watson, (1990), Deep Water Renewal in the North Atlantic. *Nature*, **6269**, 848-850.

Bryan, F. O., M. W. Hecht, and R. D. Smith, (2007), Resolution Convergence and Sensitivity Studies with North Atlantic Circulation Models. Part I: The Western Boundary Current System, *Ocean Modelling*, **16**, 3-4, 141-159.

Hecht M. W., and R. D. Smith (2008), Towards a Physical Understanding of the North Atlantic: A Review of Model Studies in an Eddying Regime, Ocean Modeling in an Eddying Regime, Geophysical Monograph Series, AGU, Hecht and Hasumi Eds.

Gerdes, R., and C. Köberle (1995), On the influence of DSOW in a numerical model of the North Atlantic general circulation. *J. Phys. Oceanogr.*, **25**, 2624-2641.

Griffies, S. M. (2010), Elements of MOM4p1, NOAA/GFDL Technical Report No. 6. NOAA/GFDL, Princeton, USA, 444 pages.

Johnson, H. L., and D. P. Marshall (2002), A theory for the surface Atlantic response to thermohaline variability, *J. Phys. Oceanogr.*, **32**, 1121-1132.

Joyce, T. M., Y.-O. Kwon, and L. Yu, (2009), On the Relationship between Synoptic Wintertime Atmospheric Variability and Path Shifts in the Gulf Stream and the Kuroshio Extension, *J. Climate*, **22**, 3177-3192.

Joyce, T. M., and R. Zhang (2010), On the path of the Gulf Stream and the Atlantic Meridional overturning circulation. *J. Climate*, **23**, doi:10.1175/2010JCLI3310.1.

Kanzow, T. et al. (2010) Seasonal variability of the Atlantic meridional overturning circulation at 26.5°N. *J. Climate*, **21**, doi:10.1175/2010JCLI3389.1.

Kawase, M. (1987), Establishment of deep ocean circulation driven by deep?water production, *J. Phys. Oceanogr.*, **17**, 2294-2317.

Lumpkin, R. and K. Speer, (2007) Global Ocean Meridional Overturning, *J. Phys. Oceanogr.*, **37**, 2550-2562.

Minobe, S., A. K. Yoshida, N. Komori, S. P. Xie, and R. J. Small, 2008, Influence of the Gulf Stream on the troposphere, Nature, 452, 206-209.

Molinari, R. L., Z. Garraffo, and D. Snowden (2008), Differences between observed and a coupled simulation of North Atlantic sea surface currents and temperature, *J. Geophys. Res.*, **113**, C09011, doi:10.1029/2008JC004848.

Peña-Molino, B., and T. M. Joyce (2008), Variability in the Slope Water and its relation to the Gulf Stream path. *Geophys. Res. Lett.*, **35**, L03606, doi:10.1029/2007GL032183.

Putman, W. M., and S. -J. Lin (2007), Finite-volume transport on various cubed-sphere grids. *J. Comput. Phys.*, **227**, 55-78.

Roberts M. J. and R. A. Wood (1997), Topographic Sensitivity Studies with a Bryan-Cox-Type Ocean Model. *J. Phys. Oceanogr.*, **27**, 823-836.

Smith, R. D., M. E. Maltrud, F. O. Bryan, and M. W. Hecht, (2000), Numerical simulation of the North Atlantic ocean at $1/10°$. *J. Phys. Oceanogr.*, **30**, 1532-1561.

Toole, J. M., R. G. Curry, T. M. Joyce, M. MacCartney and B. Peña-Molino (2010), Transport of the North Atlantic Deep Western Boundary Current About 39°N, 70°W: 2004-2008, *Deep Sea Research II*, In Press.

Weese, S. R., and F. O. Bryan, (2006), Climate impacts of systematic errors in the simulation of the path of the North Atlantic Current, *Geophys. Res. Lett.*, **33**, L19708, doi:10.1029/2006GL027669.

Winton, M., R. W. Hallberg, and A. Gnanadesikan (1998), Simulation of density-driven frictional downslope flow in z-coordinate ocean models. *J. Phys. Oceanogr.*, **28**, 2163-2174.

Yeager, S. G., and M. Jochum (2009), The connection between Labrador Sea buoyancy loss, deep western boundary current strength, and Gulf Stream path in an ocean circulation model. *Ocean Modelling*, **30**, 207-224, doi:10.1016/j.ocemod.2009.06.014.

Zhang, R. and G. K. Vallis (2007), The role of bottom vortex stretching on the path of the North Atlantic Western Boundary Current and on the Northern Recirculation Gyre. *J. Phys. Oceanogr.*, **27**, 2053-2080.

Zhang, R. (2008), Coherent surface-subsurface fingerprint of the Atlantic meridional overturning circulation, *Geophys. Res. Lett.*, **35**, L20705, doi:10.1029/2008GL035463.

Zhang, R., (2010), Latitudinal dependence of Atlantic Meridional Overturning Circulation (AMOC) variations. *Geophys. Res. Lett.*, **37**, L16703, doi:10.1029/2010GL044474.

Figure captions

1. Bathymetry of the North Atlantic used in GFDL CM2.5 for the control and the perturbed experiments. (a) Control experiment C1 (b) Perturbed experiment P1 (c) Control experiment C2 (d) Perturbed experiment P2. In the perturbed experiments the bathymetry in the area within the thick black frame is deepened by 300m, whenever the background ocean depth in this area in the control experiments is more than 300m.

2. The difference of the annual mean deep flow (u,v) at 3000m between the perturbed experiment P1 and the control experiment C1 of year 1 (a) and year 5 (b) respectively.

3. The difference of the annual mean AMOC (Sv) between the perturbed and the control experiments at the potential density level $1036.9 kg/m^3$ as a function of latitude for the first 10 years. (a) Absolute AMOC difference $(P1-C1)$ (b) Absolute AMOC difference $(P2-C2)$ (c) Relative AMOC difference, i.e. $(P1-C1)$ minus the 10-year mean difference $(\overline{P1}-\overline{C1})$ at each latitude, (d) Relative AMOC difference, i.e. $(P2-C2)$ minus the 10-year mean difference $(\overline{P2}-\overline{C2})$ at each latitude.

4. Annual mean passive dye tracer at deep ocean (3000m) (a,b,c) and barotropic streamfunction (Sv) (d,e,f) for year 2,4,6 of the perturbed experiment (P1).

5. Annual mean age tracer (year), passive dye tracer released from the Denmark Strait, and horizontal velocities (u,v, m/s) in the North Atlantic deep ocean (average of 2500m to 4000m) averaged from year 6 to 10 of the control experiment C1 (a,c) and the perturbed experiment P1 (b,d) in CM2.5.

6. Annual mean Atlantic meridional overturning streamfunction (Sv) averaged from year 6 to 10 of the control experiment C1 (a) and the perturbed experiment (b) in CM2.5.

7. Annual mean North Atlantic barotropic streamfunction (Sv), SST (K), and upper ocean (100m) horizontal velocities (u,v, m/s) averaged from year 6 to 10 of the control experiment C1 (a,c) and the perturbed experiment P1 (b,d) in CM2.5.

8. Annual mean differences between the Perturbed and Control Experiments ($P1-C1$) averaged from year 6 to 10 of in CM2.5 for (a) North Atlantic barotropic streamfunction and (b) SST, both overlapped with the differences in the upper ocean (100m) horizontal velocities (u,v).

9. Simulated annual mean Gulf Stream and North Atlantic Current in CM2.5 averaged from year 6 to 10 of the control experiment C1 (a,c) and the perturbed experiment P1 (b,d). (a,b) Zonal velocity (m/s) at section 60°W, (c,d) Meridional velocity (m/s) at section 46°N. Note the contour interval is 0.02m/s in (a,c) and 0.04m/s in (b,d).

10. Simulated Eddy Kinetic Energy (EKE) (cm^2s^{-2}) of the surface geostrophic flow and the rms SSH variability (cm) averaged from year 6 to 10 of the control experiment C1 (a,d) and the perturbed experiment P1 (b,e) in CM2.5, and the comparison with observations - the merged altimeter product for the period of 2002-2006 (c,f). Both simulated and observed EKE and rms SSH variability are derived from 7-day snapshots of SSH field. The EKE is derived from SSH through geostrophy and plotted in logarithmic scale. The altimeter products were produced by SSALTO/DUACS and distributed by AVISO with support from CNES.

11. Nordic Sea surface density change (Kg/m^3) in February averaged between two 5-year periods (year 16-20 minus year 6-10). (a) Perturbed experiment P1 (b) Control experiment C1

Dynamic content captions

1. Animation (3-dim) of annual mean passive dye tracer released from the Denmark Strait for year 1 to 10 of the perturbed experiment P1. The thick black lines mark ocean isodepth contours at 1000m, 2000m, 3000m.

2. Animation (3-dim) of annual mean passive dye tracer released from the Denmark Strait for year 1 to 10 of the control experiment C1. The thick black lines mark ocean isodepth contours at 1000m, 2000m, 3000m.

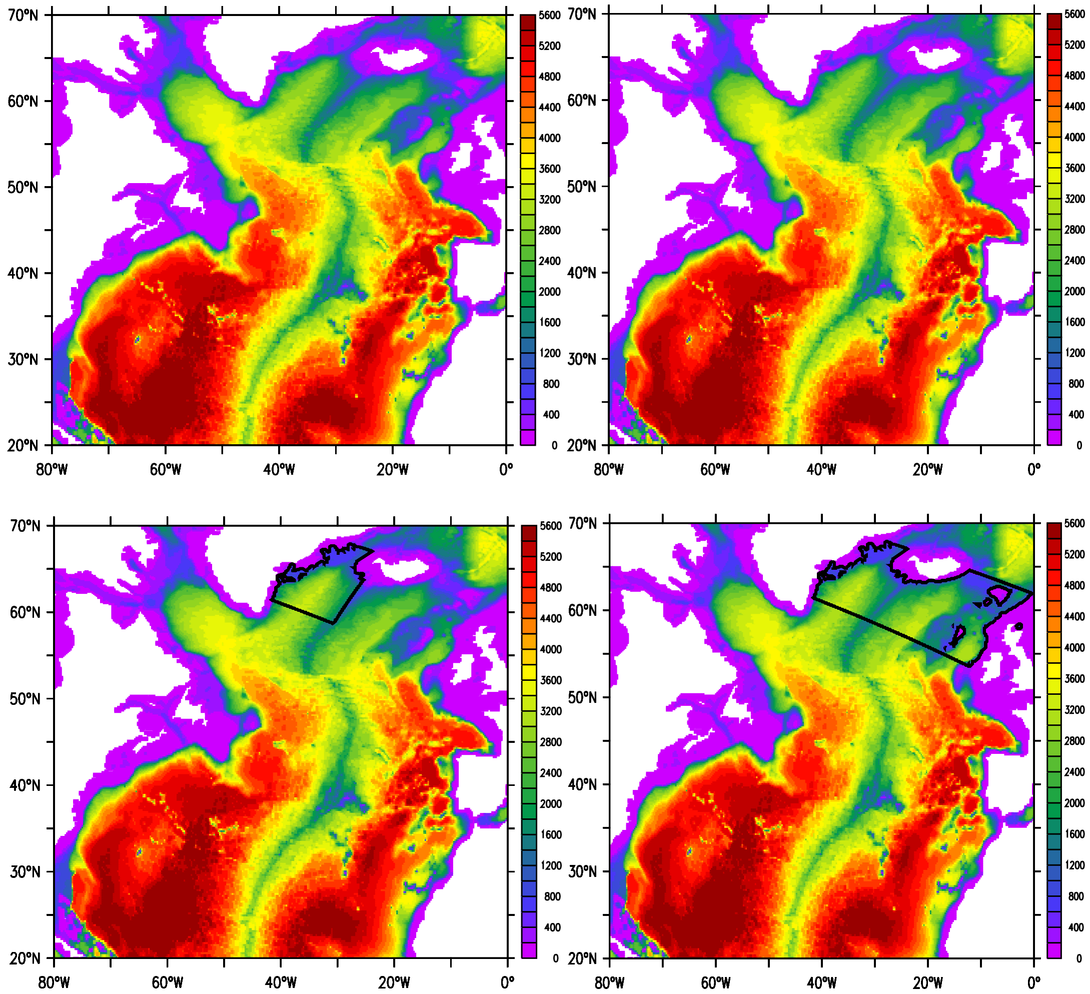
70°N
60°N
50°N
40°N
30°N
20°N
80°W
60°W
40°W
20°W
0°
5600
5200
4800
4400
4000
3600
3200
2800
2400
2000
1600
1200
800
400
0

Figure 1

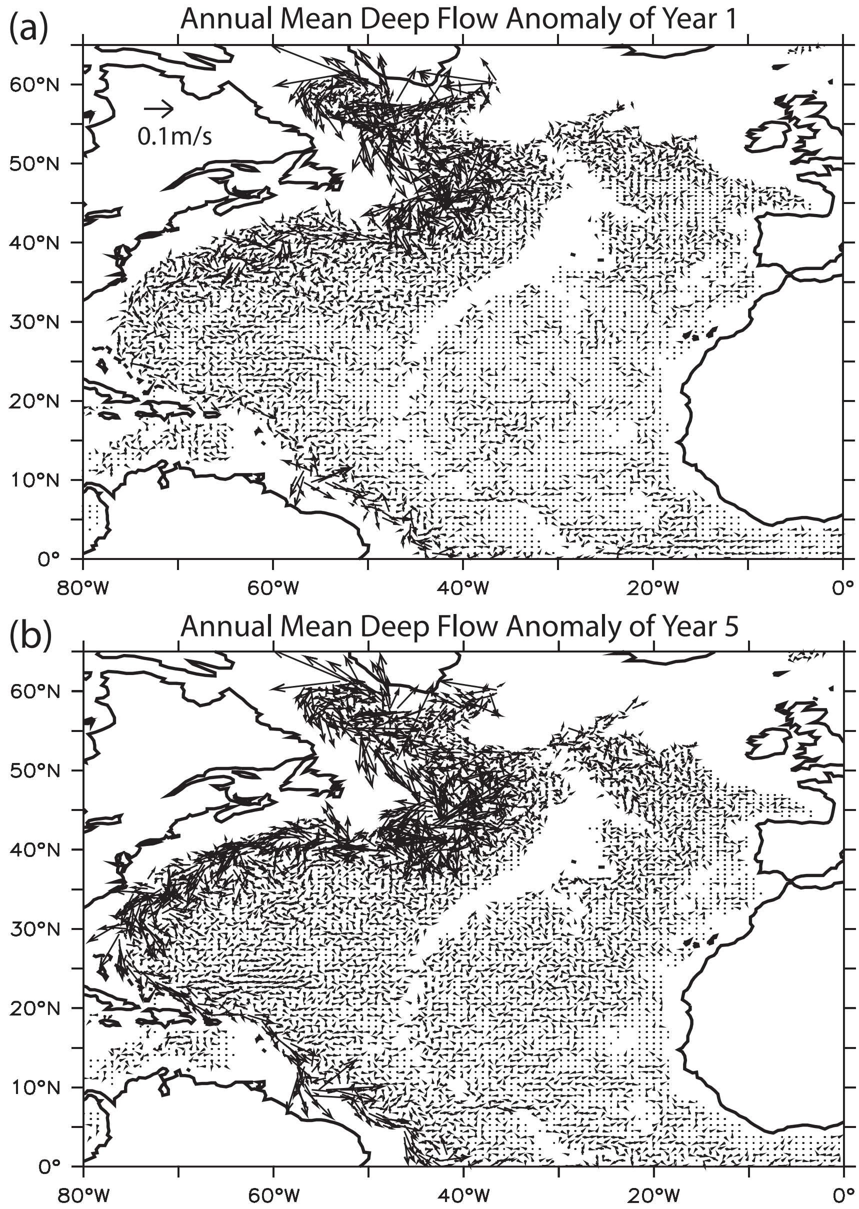
(a)
Annual Mean Deep Flow Anomaly of Year 1
0.1m/s
60°N
50°N
40°N
30°N
20°N
10°N
0°
80°W
60°W
40°W
20°W
0°
(b)
Annual Mean Deep Flow Anomaly of Year 5
60°N
50°N
40°N
30°N
20°N
10°N
0°
80°W
60°W
40°W
20°W
0°

Figure 2

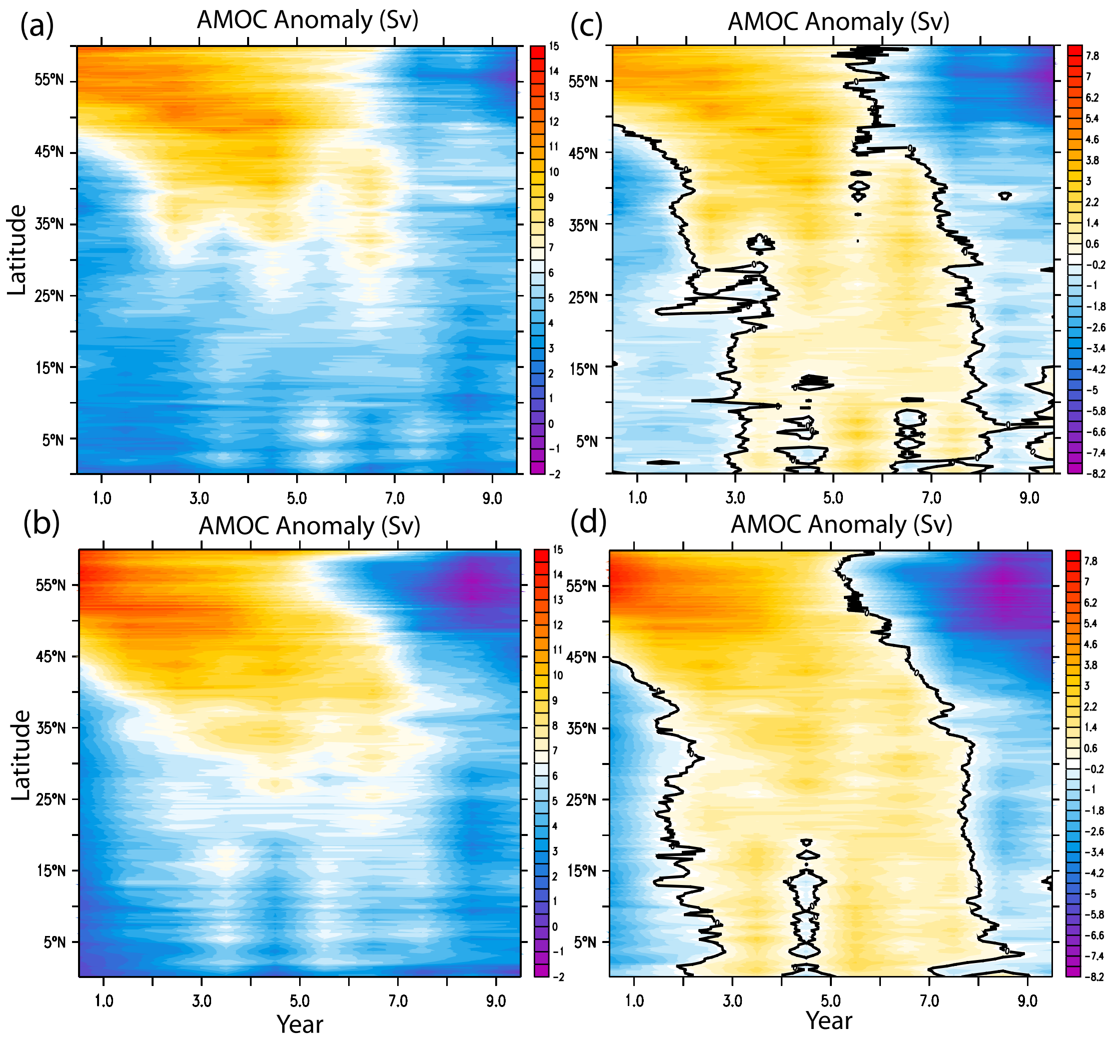
(a)
AMOC Anomaly (Sv)
(b)
AMOC Anomaly (Sv)
(c)
AMOC Anomaly (Sv)
(d)
AMOC Anomaly (Sv)
Latitude
Year
55°N
45°N
35°N
25°N
15°N
5°N
1.0
3.0
5.0
7.0
9.0

Figure 3

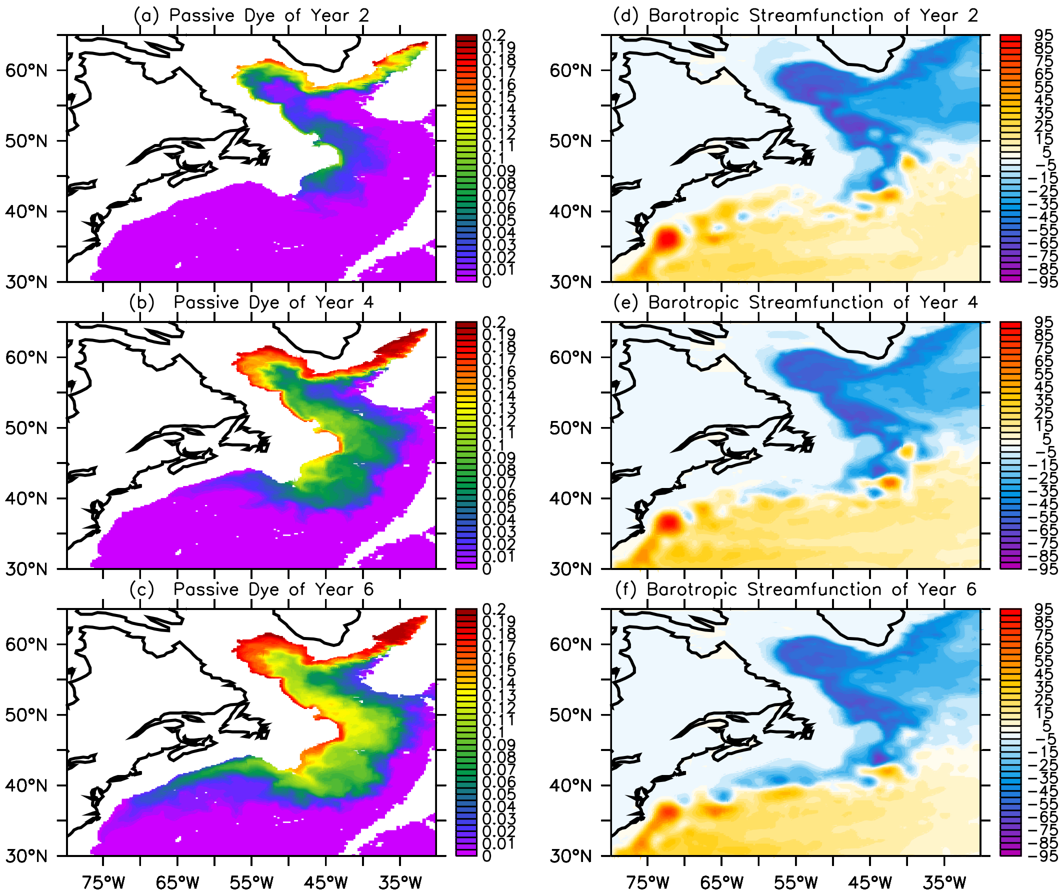
(a) Passive Dye of Year 2
(b) Passive Dye of Year 4
(c) Passive Dye of Year 6
(d) Barotropic Streamfunction of Year 2
(e) Barotropic Streamfunction of Year 4
(f) Barotropic Streamfunction of Year 6
60°N
50°N
40°N
30°N
75°W
65°W
55°W
45°W
35°W

Figure 4

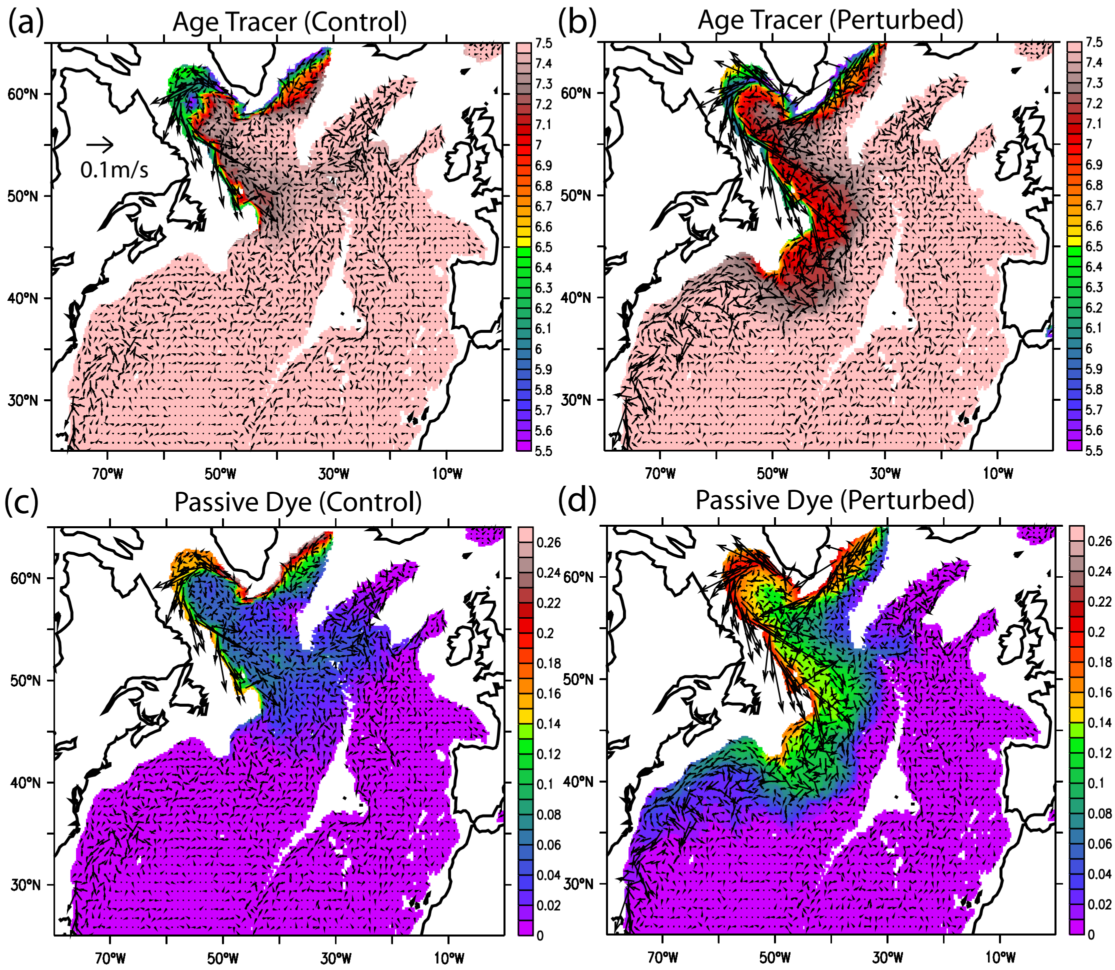
(a)
Age Tracer (Control)
(b)
Age Tracer (Perturbed)
(c)
Passive Dye (Control)
(d)
Passive Dye (Perturbed)
0.1m/s
60°N
50°N
40°N
30°N
70°W
50°W
30°W
10°W
7.5
7.4
7.3
7.2
7.1
7
6.9
6.8
6.7
6.6
6.5
6.4
6.3
6.2
6.1
6
5.9
5.8
5.7
5.6
5.5
0.26
0.24
0.22
0.2
0.18
0.16
0.14
0.12
0.1
0.08
0.06
0.04
0.02
0

Figure 5

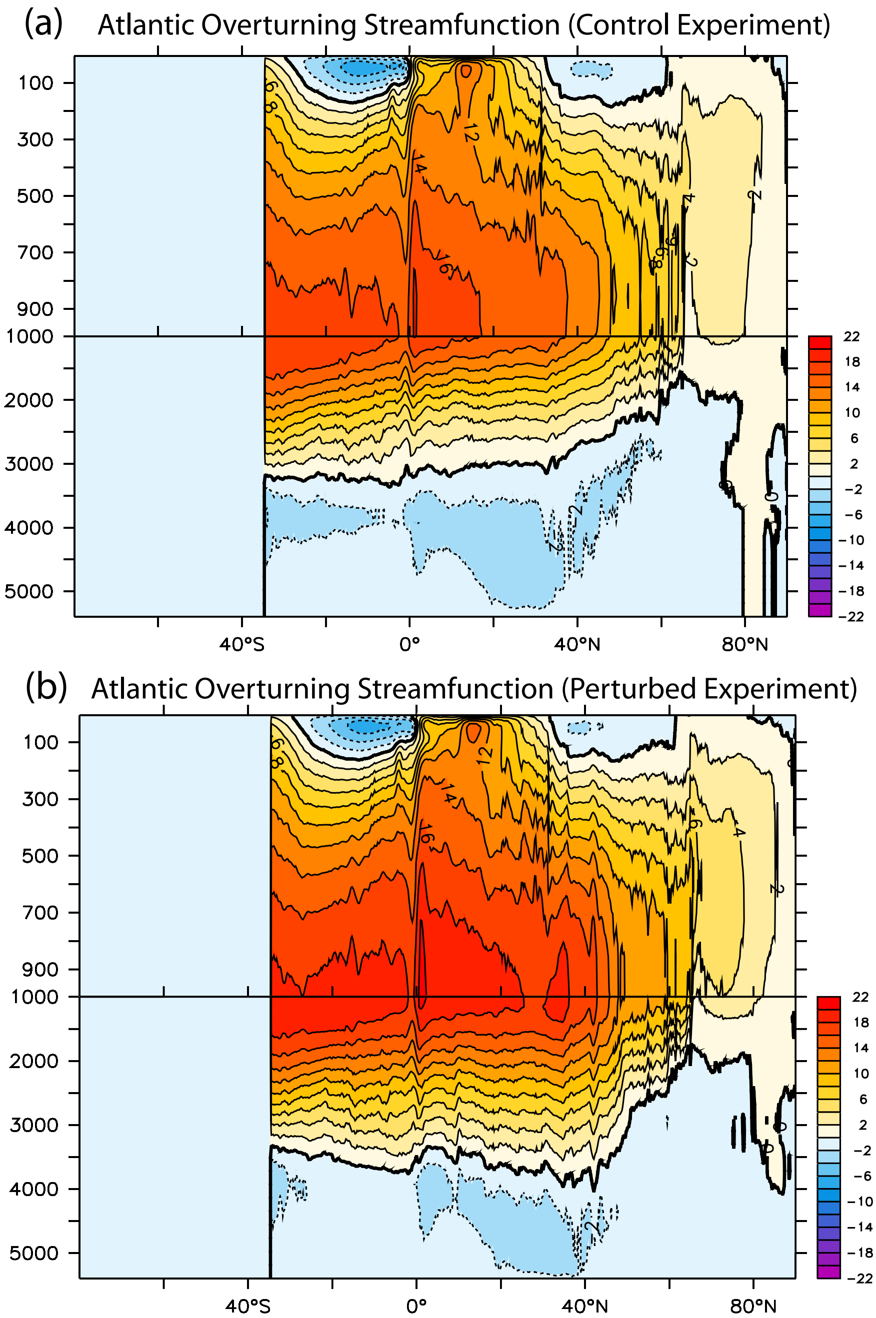
(a) Atlantic Overturning Streamfunction (Control Experiment)
100
300
500
700
900
1000
2000
3000
4000
5000
40°S
0°
40°N
80°N
22
18
14
10
6
2
−2
−6
−10
−14
−18
−22
(b) Atlantic Overturning Streamfunction (Perturbed Experiment)

Figure 6

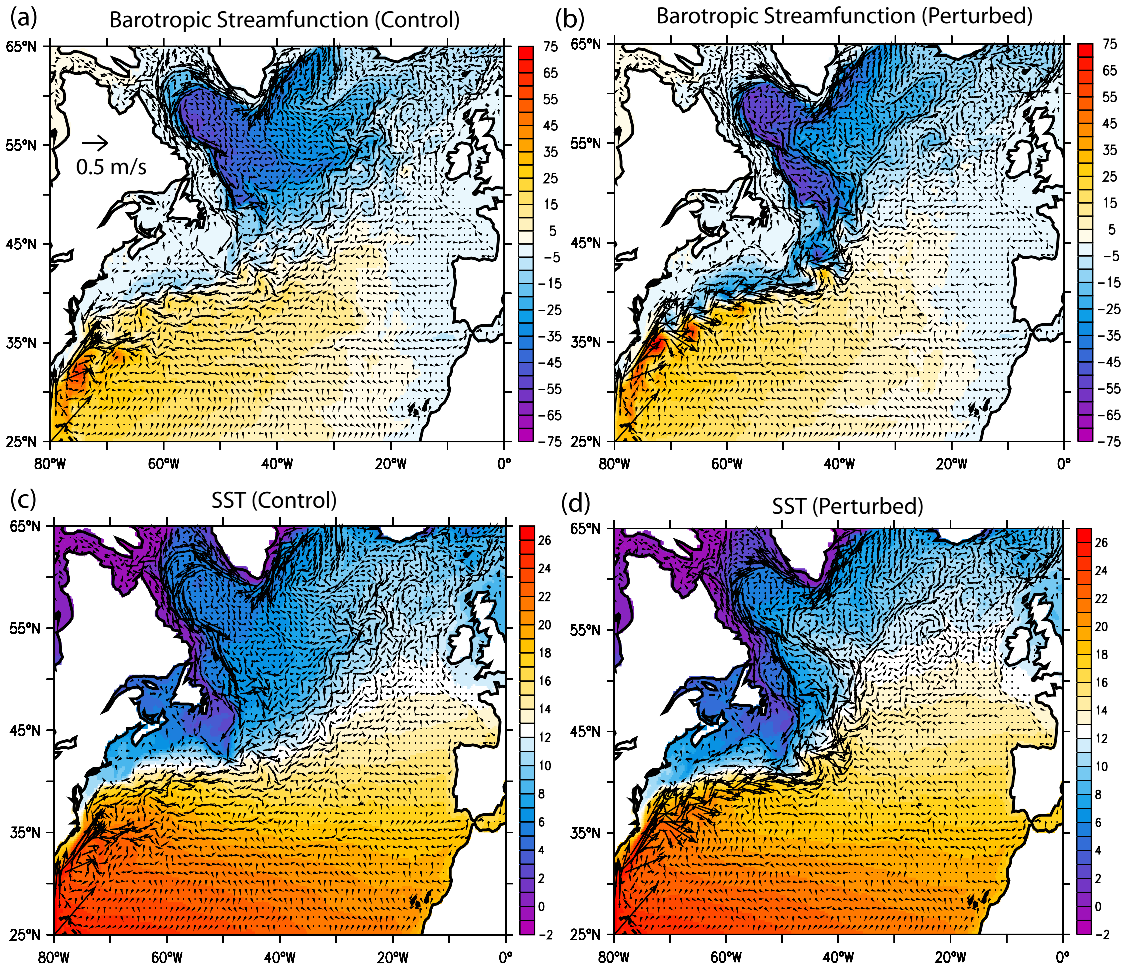
(a)
Barotropic Streamfunction (Control)
(b)
Barotropic Streamfunction (Perturbed)
0.5 m/s
(c)
SST (Control)
(d)
SST (Perturbed)
65°N
55°N
45°N
35°N
25°N
80°W
60°W
40°W
20°W
0°
75
65
55
45
35
25
15
5
−5
−15
−25
−35
−45
−55
−65
−75
26
24
22
20
18
16
14
12
10
8
6
4
2
0
-2

Figure 7

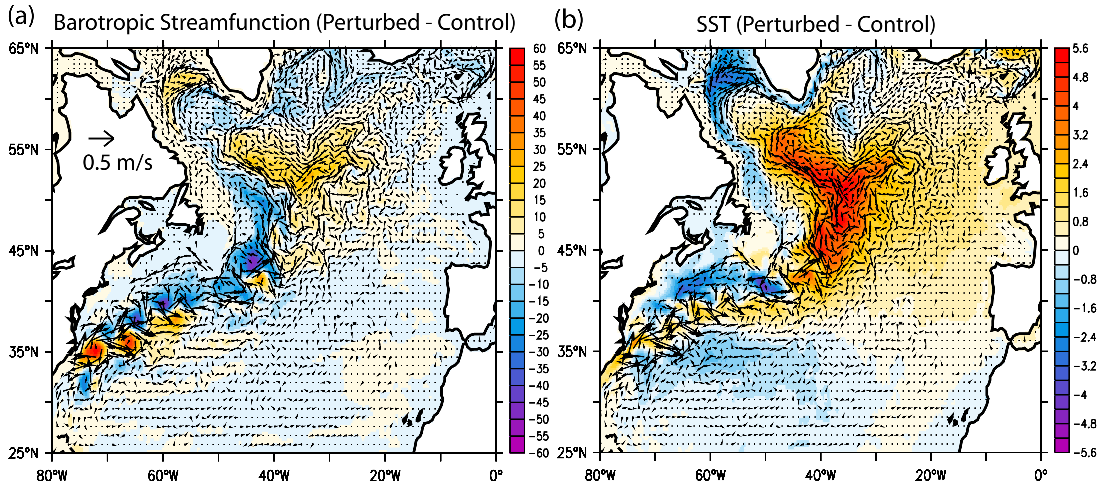
(a) Barotropic Streamfunction (Perturbed - Control)
0.5 m/s
65°N
55°N
45°N
35°N
25°N
80°W
60°W
40°W
20°W
0°
60
55
50
45
40
35
30
25
20
15
10
5
0
−5
−10
−15
−20
−25
−30
−35
−40
−45
−50
−55
−60
(b) SST (Perturbed - Control)
5.6
4.8
4
3.2
2.4
1.6
0.8
0
−0.8
−1.6
−2.4
−3.2
−4
−4.8
−5.6

Figure 8

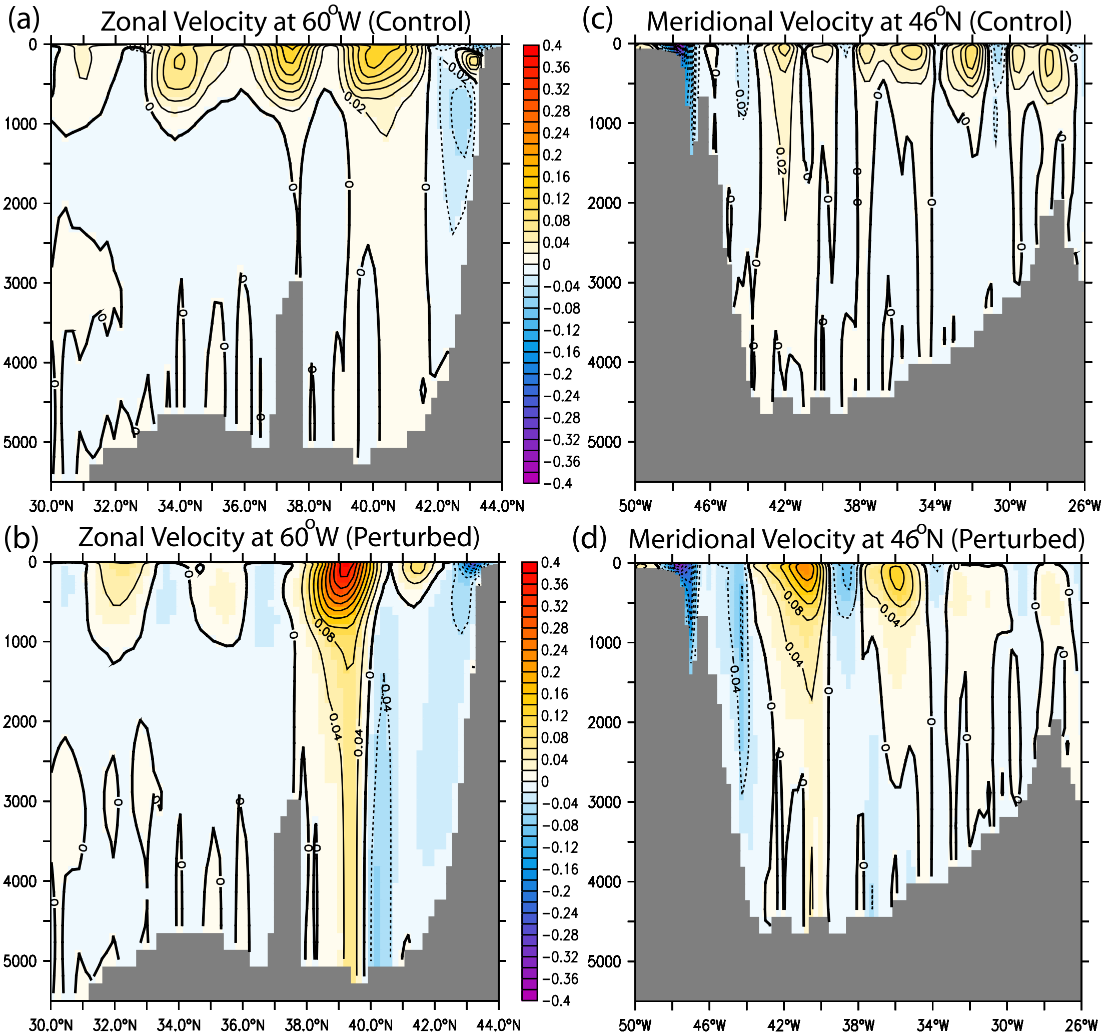
(a) Zonal Velocity at 60°W (Control)
(b) Zonal Velocity at 60°W (Perturbed)
(c) Meridional Velocity at 46°N (Control)
(d) Meridional Velocity at 46°N (Perturbed)
30.0°N
32.0°N
34.0°N
36.0°N
38.0°N
40.0°N
42.0°N
44.0°N
50°W
46°W
42°W
38°W
34°W
30°W
26°W
0
1000
2000
3000
4000
5000
0.4
0.36
0.32
0.28
0.24
0.2
0.16
0.12
0.08
0.04
0
−0.04
−0.08
−0.12
−0.16
−0.2
−0.24
−0.28
−0.32
−0.36
−0.4

Figure 9

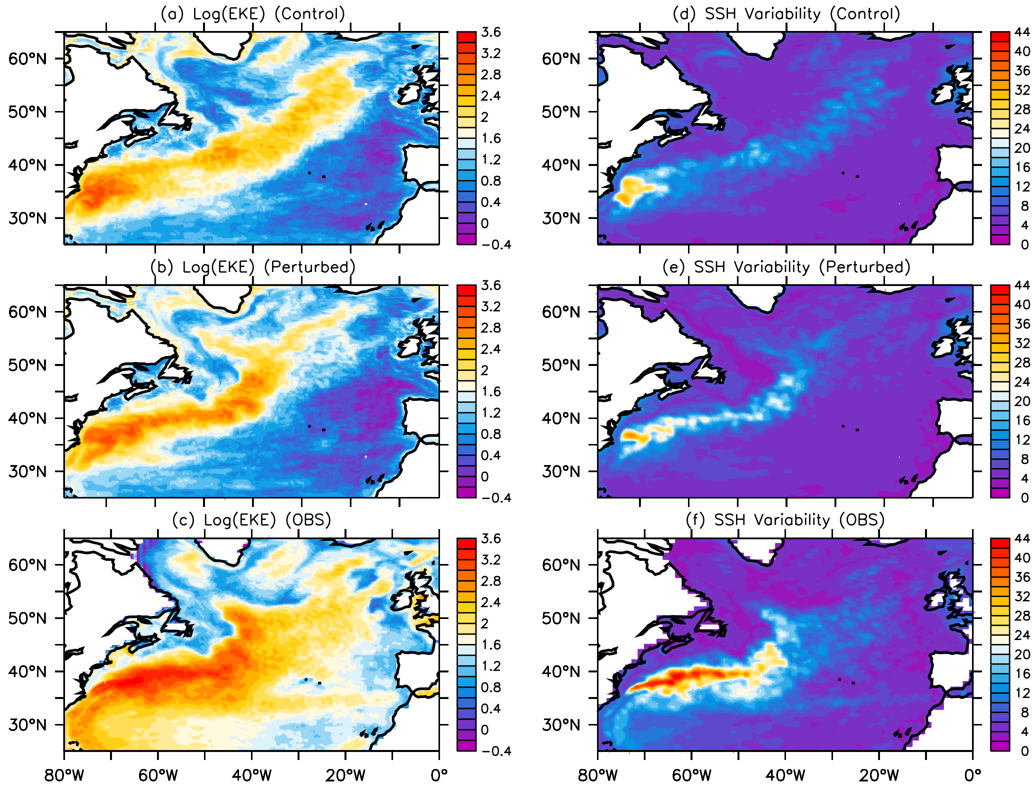
(a) Log(EKE) (Control)
(b) Log(EKE) (Perturbed)
(c) Log(EKE) (OBS)
(d) SSH Variability (Control)
(e) SSH Variability (Perturbed)
(f) SSH Variability (OBS)
60°N
50°N
40°N
30°N
80°W
60°W
40°W
20°W
0°
3.6
3.2
2.8
2.4
2
1.6
1.2
0.8
0.4
0
−0.4
44
40
36
32
28
24
20
16
12
8
4
0

Figure 10

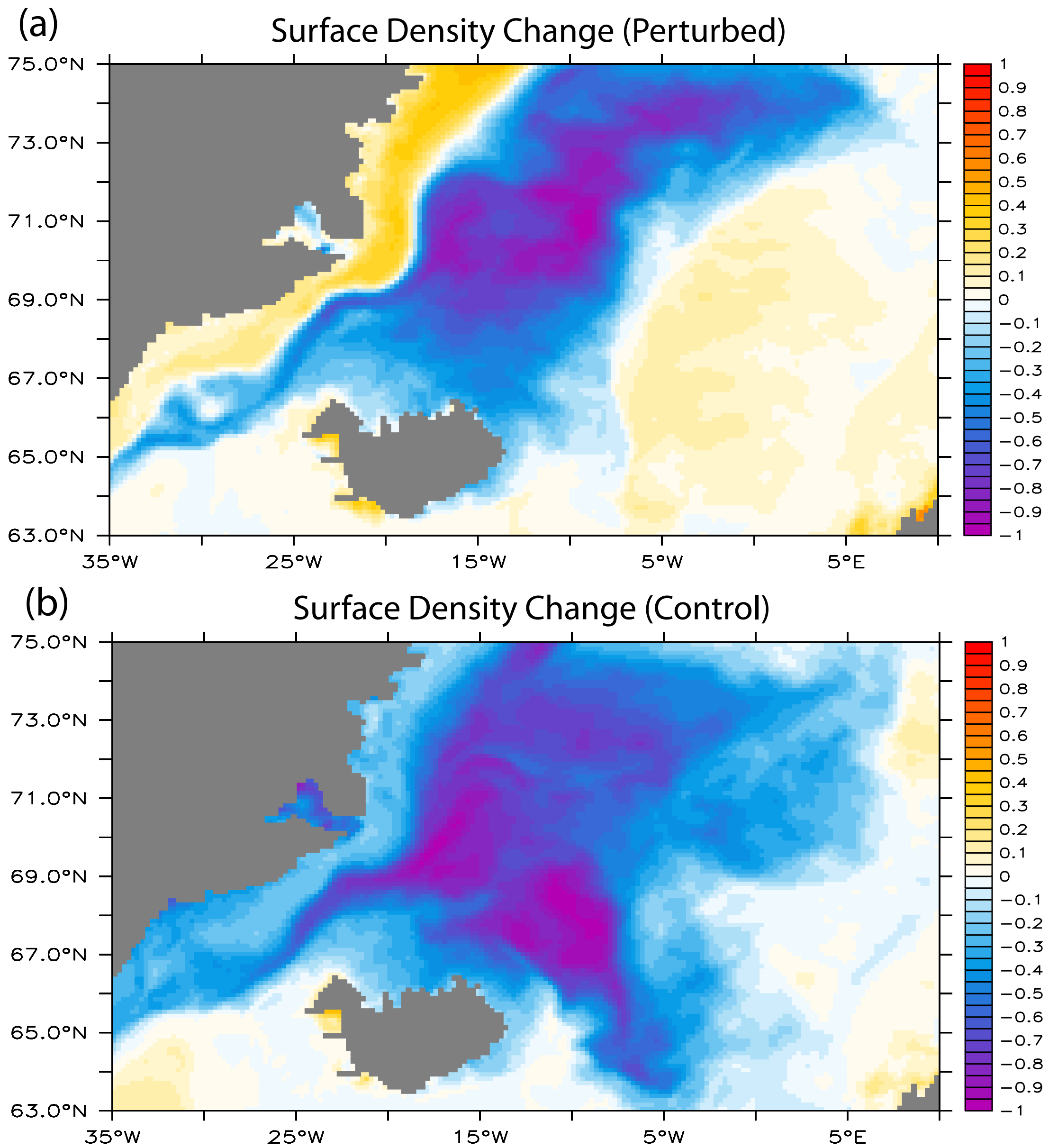
(a)
Surface Density Change (Perturbed)
75.0°N
73.0°N
71.0°N
69.0°N
67.0°N
65.0°N
63.0°N
35°W
25°W
15°W
5°W
5°E
1
0.9
0.8
0.7
0.6
0.5
0.4
0.3
0.2
0.1
0
−0.1
−0.2
−0.3
−0.4
−0.5
−0.6
−0.7
−0.8
−0.9
−1
(b)
Surface Density Change (Control)
75.0°N
73.0°N
71.0°N
69.0°N
67.0°N
65.0°N
63.0°N
35°W
25°W
15°W
5°W
5°E
1
0.9
0.8
0.7
0.6
0.5
0.4
0.3
0.2
0.1
0
−0.1
−0.2
−0.3
−0.4
−0.5
−0.6
−0.7
−0.8
−0.9
−1

Figure 11